Colloids and Surfaces B: Biointerfaces 210 (2022) 112239

Contents lists available at ScienceDirect

Colloids and Surfaces B: Biointerfaces

journal homepage: www.elsevier.com/locate/colsurfb

Interactions of hydrophilic quantum dots with defect-free and defect containing supported lipid membranes

L. Bar [a], F. Perissinotto [b], L. Redondo-Morata [b], M.I. Giannotti [c,d,e], J. Goole [f], P. Losada-Pérez [a,*]

[a] Experimental Soft Matter and Thermal Physics group (EST), Department of Physics, Université libre de Bruxelles, Boulevard du Triomphe CP223, 1050 Brussels, Belgium
[b] Université de Lille, CNRS, Inserm, CHU Lille, Institut Pasteur de Lille, U1019-UMR9017-CIIL-Centre d'Infection et d'Immunité de Lille, F-59000 Lille, France
[c] Networking Biomedical Research Networking Center on Bioengineering, Biomaterials and Nanomedicine (CIBER-BBN), Spain
[d] Nanoprobes and Nanoswitches group, Institute for Bioengineering of Catalonia (IBEC), The Barcelona Institute of Science and Technology (BIST), 08028 Barcelona, Spain
[e] Departament de Ciència dels Materials i Química Física, Universitat de Barcelona, 08028 Barcelona, Spain
[f] Laboratory of Pharmaceutics and Biopharmaceutics, Université libre de Bruxelles, Campus de la Plaine, CP 207, Boulevard du Triomphe, 1050 Brussels, Belgium

ARTICLE INFO

Keywords:
Hydrophilic quantum dots
Lipid membrane defects
Supported lipid bilayers
Quartz crystal microbalance with dissipation
Atomic force microscopy
Nanomechanics

ABSTRACT

Quantum dots (QDs) are semiconductor nanoparticles with unique optical and electronic properties, whose interest as potential nano-theranostic platforms for imaging and sensing is increasing. The design and use of QDs requires the understanding of cell-nanoparticle interactions at a microscopic and nanoscale level. Model systems such as supported lipid bilayers (SLBs) are useful, less complex platforms mimicking physico-chemical properties of cell membranes. In this work, we investigated the effect of topographical homogeneity of SLBs bearing different surface charge in the adsorption of hydrophilic QDs. Using quartz-crystal microbalance, a label-free surface sensitive technique, we show significant differences in the interactions of QDs onto homogeneous and inhomogeneous SLBs formed following different strategies. Within short time scales, QDs adsorb onto topographically homogeneous, defect-free SLBs is driven by electrostatic interactions, leading to no layer disruption. After prolonged QD exposure, the nanomechanical stability of the SLB decreases suggesting nanoparticle insertion. In the case of inhomogeneous, defect containing layers, QDs target preferentially membrane defects, driven by a subtle interplay of electrostatic and entropic effects, inducing local vesicle rupture and QD insertion at membrane edges.

1. Introduction

The potential use of nanoparticles in nanomedicine as drug/gene delivery, phototherapy and bioimaging agents depends on the understanding and control over nanoparticle-cell interactions [1,2]. The complexity of cell membranes makes artificial lipid bilayers convenient models to understand the interactions with nanoparticles at a fundamental level. Among lipid membrane models, solid-supported membranes such as supported lipid bilayers (SLBs) and supported vesicle layers (SVLs) are very useful approaches since their formation is rather straightforward, they retain in vivo membrane properties and are amenable to be studied by high resolution surface-sensitive techniques at a multiscale level [3,4]. Mechanistic understanding of the interaction of nanoparticles with model cell membranes is a subject of intensive research and entails a systematic study to dissect the role of physico-chemical parameters of both membranes and nanoparticles, i.e., chemical composition, lateral organization, nanoparticle size and shape, among others [5,6]. For instance, particles in the nano/meso scale range (50–500 nm) partition onto a different lipid phase depending on their size as a result of elastic energy minimization [7]. A very relevant property is surface charge, which is supposed to play a dominant role in early-stage nanoparticle uptake driven by long-range electrostatic interactions [8]. Yet, controversial studies regarding the effect of anionic and cationic nanoparticles (whether adsorption or insertion takes place and whether anionic or cationic charge induce more or less disruption) with oppositely charged membranes have been reported [9–11] indicating that electrostatic interactions are not the only ingredient taking part in early-stage of lipid membrane-nanoparticle interactions. From a thermodynamic viewpoint, the driving force for nanoparticle insertion into lipid membranes is dominated by the hydrophobic effect. Particles bearing hydrophobic groups in their surface functionalities minimize water-exposed hydrophobic surface area by inserting into the

* Corresponding author.

https://doi.org/10.1016/j.colsurfb.2021.112239
Received 22 September 2021; Received in revised form 17 November 2021; Accepted 18 November 2021
Available online 25 November 2021

hydrophobic bilayer core [12,13]. A parameter that influences hydrophobic interactions is membrane curvature, which itself is intimately related to membrane mechanical properties, to (local) fluctuations of the constituent lipids in membranes and to the presence of membrane defects. The latter consist of membrane unevenness which could locally modulate height, shape, or mechanical properties of the lipid bilayer. As a matter of fact, membrane defects have been shown to act as nanoparticle insertion sites by computational simulations [12,14]. Experimental studies assessing the influence of membrane defects are scarce and restricted to few works on zwitterionic lipid membranes with hydrophilic anionic Au nanoparticles and cationic quantum dots (QDs), that preferentially interact with membrane edges or domain boundaries in raft-containing membranes [15,16]. However, no information on how nanoparticle adsorption and eventual insertion on membranes affect bilayer stability and nanomechanical properties has been so far reported to the best our knowledge.

In this work, we evaluate the effect of supported lipid bilayer surface charge and topography, in particular, the influence of defects in supported lipid membrane layers such as intact vesicles or lipid bilayer exposed edges, on nanoparticle-lipid membrane interactions. We chose CdTe QDs with hydrophilic functionalization rendering the particles negatively charged in the buffer used. Specifically, we followed in real-time and in situ the formation of homogeneous and inhomogeneous DOPC, DOTAP or DOPC:DOTAP SLBs and subsequent interactions with QDs using complementary-surface-sensitive techniques, namely quartz crystal microbalance with dissipation monitoring (QCM-D) and atomic force microscopy (AFM). We use the terms homogeneous and inhomogeneous to refer to the fact that the formed SLB is topographically homogeneous or inhomogeneous. For the formation of homogeneous SLBs we employed two different methodologies, vesicle rupture and solvent exchange, and assessed the degree of QDs layer disruption by nanomechanical mapping. Inhomogeneous SLBs were obtained by vesicle adsorption and rupture onto rougher substrates. Significant differences in QD-membrane interaction QCM-D responses were observed from homogeneous and inhomogeneous supported lipid membranes. The former displayed QD adsorption and minor layer disruption or change in nanomechanical properties. In the case of inhomogeneous supported membranes, the degree of inhomogeneity was assessed using the energy dissipation provided by QCM-D as a descriptor. The larger the dissipation −and thus the amount of layer defects− , the stronger QD layer disruption, inducing vesicle rupture and QD insertion at patch boundary edges.

2. Materials and methods

2.1. Materials used

Solutions of 1,2-dioleoyl-sn-glycero-3-phosphocholine (DOPC) and 1,2-dioleoyl-3-trimethylammonium-propane (DOTAP) lipids dissolved in chloroform were purchased from Avanti Polar Lipids (Alabaster, AL, USA). TRIS buffer was prepared with TRIS base powder $\geq$ 99.8% (VWR Chemicals), KCl $\geq$ 99% (VWR Chemicals), and HCl 37% solution (VWR chemicals). The TRIS buffer solution (pH 8.0) used for the hydration of the dried lipid films was prepared by dissolving 10 mM Tris and 150 mM KCl in milliQ water with a resistivity of 18.2 MΩ cm at 25 °C (Simplicity® purification system, Merck Millipore, Overijse, Belgium). The pH was then adjusted to 8 with a 1 M HCl solution. The pH value evolution was tracked with a FiveEasy pHmeter from Mettler Toledo (Zaventem, Belgium). The buffer was then filtered with 0.2 μm-pore size PTFE membranes and stored at 4 °C until being used. Hydrophilic CdTe QDs were purchased from PlasmaChem GmbH (Berlin, Germany). The particle molecular weight is 32000 g/mol for a maximum emission wavelength of 550 ± 5 nm. The size of the QD core is 2.6 nm and they are terminated with -COOH groups, allowing them to be negatively charged at pH = 8. For QCM-D experiments, AT-cut quartz crystals with SiO_2 or Au (polycrystalline) coating (diameter 14 mm, thickness 0.3 mm, quoted surface roughness < 2 nm, and resonant frequency 4.95 MHz) were used as solid surfaces and purchased from Quartz Pro AB (Jarfalla, Sweden). For imaging supported lipid bilayers using AFM, the above mentioned SiO_2-coated quartz flat crystals as well as single crystal SiO_2 surfaces with (100) orientation and roughness (RMS) $r = 0.13 \pm 0.04$ nm were used. The latter were purchased from Prime Wafers (Bergschenhoek, The Netherlands).

2.2. Lipid vesicle and QD solution preparation

Commercial solutions of DOPC, DOTAP, and a prepared mixture of DOPC:DOTAP (molar ratio 1:1) in chloroform were dried under a continuous mild flow of N_2. To avoid any residues of solvent, the lipid films were kept under low pressure overnight. The films were then hydrated with fresh filtered TRIS buffer to 2 mg/mL under continuous stirring for 45 min, in a temperature-controlled water bath at $T = 37$ °C (well above the melting temperatures of DOPC $T_m \sim -16.5$ °C [17] and DOTAP $T_m = 11.5$ °C [18]). Unilamellar vesicles were formed by extrusion through polycarbonate filters with pore size 100 nm for 25 passes. The extruded solutions were then diluted in TRIS buffer for obtaining a working concentration of 0.5 mg/mL.

QDs dispersions were freshly prepared prior to each experiment. For this purpose, QDs (in powder form) were dispersed in the working buffer at 0.2 mg/mL and sonicated for 5 min just before the injection onto supported lipid layers, minimizing the probability of QD aggregation.

2.3. Solvent assisted lipid bilayer formation

A recently developed method based on solvent exchange and termed solvent assisted lipid bilayer (SALB) formation has emerged as a versatile alternative for forming supported lipid bilayers on diverse material substrates such as SiO_2 [19] and Au [20,21]. SALB does not require the formation of lipid vesicles and enables fabricating SLBs on substrates that do not possess strong enough adhesion energy for promoting the rupture of vesicles [22]. During SALB the lipid molecules are dissolved in an organic solvent and the solvent is exchanged by an aqueous buffer at low controlled rate. Upon solvent exchange, the lipid molecules undergo a series of lyotropic phase transitions (monomers, micelles, vesicles) in the bulk. After the solvent exchange process is completed, lipid vesicles in the bulk coexist with SLBs formed at the solid–liquid interface. As thoroughly reviewed by Cho and co-workers, successful SLB formation requires an optimized choice of the organic solvent, the lipid concentration and the flow rate [19]. Based on previous reported results we have used a flow rate of 100 μL/min and 0.5 mg/mL lipid concentration in isopropanol. In our experiments, lipids dissolved in chloroform were dried and redissolved in isopropanol.

2.4. Dynamic light scattering and zeta potential measurements

Vesicle diameters, polydispersity, and zeta potential ζ were determined by means of dynamic light scattering (DLS) (Malvern Zetasizer Nano ZS, Malvern, UK). The values of these parameters for the systems under study are displayed in Table S1 in the Supplementary Material.

The mean diameters of vesicles consisting of pure DOPC, pure DOTAP, and DOPC:DOTAP mixtures range between 112 and 125 nm, and the maximum recorded polydispersity value is 0.18 suggesting that vesicle dispersions are rather homogeneous in size. As expected, the zeta-potential values indicate that DOPC vesicles are zwitterionic in the used buffer, while both DOTAP and DOPC:DOTAP vesicles are positively charged, the former bearing a stronger positive charge. The CdTe QDs diameter was estimated to be $d \sim 7$ nm, which is consistent regarding the core size and the functionalization groups, and their zeta potential in the used buffer $\zeta \sim -24$ mV as obtained from DLS measurements.

2.5. Quartz crystal microbalance with dissipation monitoring

QCM-D measurements were carried out in a Qsense E4 instrument (Biolin Scientific, Gothenburg, Sweden), which enables simultaneous monitoring of frequency and dissipation changes, $\Delta f/n$ and ΔD, with n the overtone number. SiO_2-coated quartz sensors were cleaned by immersion for 2 h in a solution of 2% sodium dodecyl sulfate (SDS) in milli-Q water, then rinsed in milli-Q water and dried with N_2. The Au-coated quartz sensors were cleaned by immersion for 5 min in a 5:1:1 mixture of milli-Q water, ammonia and hydrogen peroxide heated at 75 °C, then rinsed in milli-Q water and dried with N_2. Shortly prior to the beginning of the QCM-D measurements, the sensors were exposed to UV-light using a UV-ozone cleaner (Bioforce Nanosciences, Wetzlar, Germany) for 15 min and their water contact angle measured before their introduction into the QCM-D modules. The changes in $\Delta f/n$ and ΔD were monitored at five different overtones (from 3rd to 11th) and QCM-D experiments were performed at 37 ± 0.02 °C.

The experiments were carried out as follows. First, a baseline with pure TRIS buffer was established. Lipid vesicles were then injected over the different types of sensor chips. After reaching a stable supported lipid membrane layer, a rinsing step with buffer was performed, followed by the addition of CdTe QDs. All additions were carried out at a flow rate of 50 μL/min. For the SALB experiments, a baseline was firstly established in buffer during 10–15 min. Afterwards, TRIS buffer was exchanged with pure isopropanol until complete solvent exchange takes place and a new stable baseline is achieved. Then, the lipids dissolved in isopropanol at 0.5 mg/mL were injected for 15 min, followed by TRIS buffer replacement for 15 min. All the injections were carried out at a flow rate of 100 μL/min.

2.6. Atomic force microscopy (AFM)

AFM quantitative imaging (QI) and force spectroscopy measurements were performed using a Nanowizard 3 AFM (Bruker, Nano GmbH, Berlin, Germany). All the measurements were performed in TRIS buffer (10 mM TRIS, 150 mM KCl, pH 8) at room temperature. Triangular silicon nitride MLCT-F cantilevers (Bruker, Nano GmbH, Berlin, Germany) with quoted cantilever length of $L \sim 85$ μm, resonance frequency $f \sim 125$ kHz, nominal spring constant k ~ 0.6 N/m and nominal tip radius of 20 nm were used. The AFM cantilever was calibrated in buffer against a clean glass slide [23]. For AFM measurements, SLB samples were always kept hydrated and transferred from the QCM-D modules to the AFM liquid cell to minimize possible dewetting. QI images were taken at different scan sizes using a pixel sampling of 200 × 200, cantilever speed of 25 μm/s, and setpoint force of 500 pN. Force mapping was recorded by using a force setpoint of 5 nN and approach speed of 1.0 μm/s. AFM measurements were carried out at room temperature ($T \sim 20$ °C) keeping the volume of the buffer constant. Samples for which time-dependent measurements were carried out were kept hydrated in the dark at $T \sim 20$ °C.

2.7. Contact angle measurements

Water contact angle (WCA) measurements were carried out using an Attension ThetaLite (Biolin Scientific, Gothenburg, Sweden) based on the sessile drop method. A small drop (3 μL) of milli-Q water was deposited onto clean, UV-ozone treated flat SiO_2-coated and Au-coated sensors and the shape of the drop formed on the surface was evaluated. The contact angle of a 3 μL droplet of ultrapure water was measured for 10 s using a recording speed of 20 frames/s. All water contact angles (WCA) were measured at room temperature. Both surfaces were hydrophilic with WCA values between 25° and 34° for Au surfaces, and < 5° for SiO_2 surfaces.

3. Results and discussion

3.1. QDs interactions with homogeneous -defect free- supported lipid bilayers

Supported lipid bilayers (SLBs) of zwitterionic DOPC, positively charged DOTAP, and an equimolar mixture DOPC:DOTAP were formed on flat SiO_2-coated quartz crystal sensors using two different methodologies: i) vesicle adsorption and rupture (VAR), ii) solvent exchange (SALB). Fig. 1 shows the QCM-D frequency and dissipation changes of the 9th overtone, $\Delta f/n$ and ΔD, during the VAR and SALB processes on SiO_2 surfaces, followed by the addition of hydrophilic CdTe QDs. Let us start by discussing the formation of SLBs by VAR (Fig. 1 A, B, panels labelled as 1), whose pathway depends strongly on the electrostatic interactions between the underlying solid surface and the vesicles. In the case of zwitterionic DOPC vesicles, the formation of SLBs requires a critical number of vesicles adsorbed on SiO_2, as reflected in the mininum in the $\Delta f/n$ signal (maximum in ΔD). After adsorption to SiO_2, the frequency shift signal increases (mass loss) and the dissipation decreases back reaching small plateau values, indicating that vesicles fuse and rupture releasing the entrapped water and forming a thin and rigid bilayer, as previously reported in the literature [24,25]. In our measurements, rupture took place reaching small $\Delta f/n$ and ΔD plateau values, followed by a slow and continuous decrease in frequency and increase in dissipation, most likely due to layer restructuration and continuous adsorption of few vesicles that could still be present in the bulk, as observed in previous vesicle adsorption and rupture studies [26]. Upon addition of DOPC:DOTAP vesicles the SLB formation pathway changes, displaying smaller values of $\Delta f/n$ minimum (ΔD maximum) and thus less contacts between adhered vesicles being necessary to yield rupture. For pure DOTAP vesicles, instead of displaying a maximum, $\Delta f/n$ decreases monotonically reaching plateau values consistent with the formation of a homogeneous lipid bilayer, $\Delta f/n \sim -25$ Hz and $\Delta D < 1{\cdot}10^{-6}$ [26] (see Table S2 in the Supplementary Material). DOTAP vesicles are positively charged (largest zeta potential) and their rupture takes place spontaneously upon adsorption driven by the strong electrostatic interaction with the SiO_2 surface.

Panels C and D in Fig. 1 display the $\Delta f/n$ and ΔD responses during the SALB process and subsequent addition of QDs. A complete overview of the SALB process by QCM-D can be found in Fig. S1 of the Supplementary Material. For the sake of better display, we have restricted ourselves to the steps that involve the addition of lipids dissolved in isopropanol and the subsequent exchange of isopropanol by the TRIS buffer. The former shows a small decrease in frequency ($\Delta f/n \sim -4.1 \pm 0.2$ Hz) equivalent to the adsorption of lipid monomers at the solid-buffer interface, while for the latter the resulting $\Delta f/n$ and ΔD plateaus are consistent with homogeneous SLBs and agree well with their VAR counterparts (see Table S2 in the Supplementary Material). We have used the ΔD values and the overtone dispersion as benchmarks for evaluating the degree of homogeneity of the formed supported bilayers. For both layers formed by VAR and SALB $\Delta D \leq 1{\cdot}10^{-6}$ and overtones overlap for $\Delta f/n$ and ΔD final plateaus (example in Fig. S1) indicating that the resulting layers are homogeneous.

After the formation of the supported lipid bilayers, a solution of 0.2 mg/mL hydrophilic, -COOH-terminated CdTe QDs in TRIS buffer (10 mM TRIS, 150 mM KCl, pH 8) was injected over the sensor surfaces with a rate of 50 μL/min for 10 min. For a better comparison of the different QDs-lipid layers interactions, time, $\Delta f/n$ and ΔD data were reset to zero before the particle's injection (see panels labelled as 2 in Fig. 1). The QDs concentration was selected based on previous results on non-specific interactions between homogeneous SLBs formed by vesicle rupture and hydrophilic CdSe QDs [27]. The adsorption of QDs on positively charged SLBs (i.e. DOTAP and DOPC:DOTAP layers) is characterized by large changes in $\Delta f/n$ (mass increase), while the dissipation signal ΔD barely changes, indicating that QDs adsorb onto the SLBs and form rigid, non-dissipative layers. For zwitterionic DOPC bilayers, no

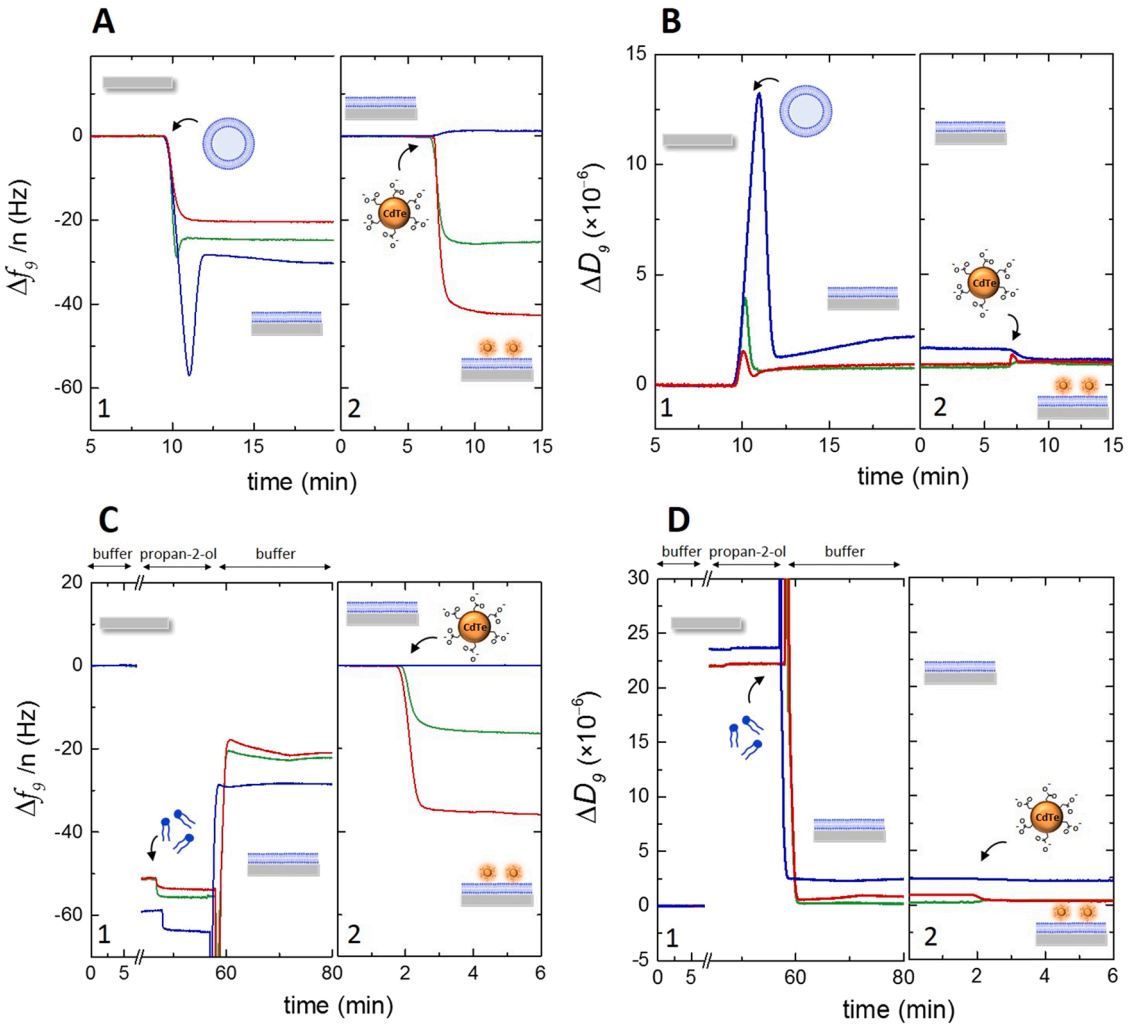

Fig. 1. Formation of homogeneous supported lipid bilayers by VAR (A, B) or SALB (C, D) on SiO_2 surfaces and subsequent interaction with hydrophilic CdTe QDs followed by QCM-D at 37 °C. Labels 1 and 2 refer to $\Delta f/n$ and ΔD changes for overtone 9 upon SLB formation (1) and CdTe QDs addition (2) on SLBs. Red solid line: pure DOTAP; blue solid line: DOPC; green solid line: DOPC:DOTAP mixture. (For interpretation of the references to colour in this figure legend, the reader is referred to the web version of this article.)

significant changes in Δf and ΔD plateau values were observed upon addition of the QDs. DOPC SLBs formed by vesicle rupture are not fully homogeneous and a slight increase in frequency (decrease in dissipation) can be detected, indicating QDs disrupt the supported membrane layer and eventually insert in the SLBs. The influence of layer inhomogeneity on QDs interactions will be assessed in Section 3.2. A complete overview of Δf and ΔD changes upon QDs addition can be found in Table 1.

The QD mass adsorbed on the SLBs was calculated using the Sauerbrey relation $\Delta m = -C\frac{\Delta f}{n}$, with C being the Sauerbrey constant $C = 17.7$ ng/cm^2 Hz [28]. The Sauerbrey relation is valid for thin, rigid layers whose oscillation is well coupled to that of quartz. In the case of pure DOTAP or DOPC:DOTAP layers, the $-\frac{\Delta D}{\Delta f/n}$ ratio observed for QDs adsorption is well below $4{\cdot}10^{-7}$ Hz, which is a well-established criterion for Sauerbrey applicability [29]. Fig. 2 depicts the QDs areal mass adsorbed as a function of the zeta potential of the original lipid vesicle suspensions. For SLBs formed by both VAR and SALB, the larger the positive surface charge, the larger adsorption, confirming that QDs adsorption is primarily driven by electrostatic interactions. The adsorption of QDs onto DOPC:DOTAP SLBs formed by SALB is less pronounced than for their VAR SLB counterparts. This difference in adsorption could be indicative of the SALB process resulting into more asymmetric bilayers. In DOPC:DOTAP mixtures, positively charged DOTAP lipid molecules are attracted to the negatively charged SiO_2 surface as compared to DOPC ones, thus resulting in an SLB where the lower leaflet has a DOPC:DOTAP molar ratio higher than 1, while the upper leaflet has a molar ratio below 1. When negative QDs are added, they are exposed to the upper leaflet, resulting in weaker interactions with the head groups present in the upper leaflet.

Table 1
Frequency and dissipation shift plateau values, $\Delta f/n$ and ΔD, for overtone 9 recorded by QCM-D after the adsorption of hydrophilic CdTe QDs onto homogeneous SLBs formed on SiO_2 sensors by VAR or SALB method.

Sample	$\Delta f/n$ $_{CdTe\ QDs}$ (Hz)		ΔD $_{CdTe\ QDs}$ ($\times 10^{-6}$)	
	VAR	SALB	VAR	SALB
DOTAP	− 39.7 ± 1.4	− 36.0 ± 1.1	− 1.0 ± 0.5	− 0.6 ± 0.4
DOPC:DOTAP	− 25.1 ± 0.3	− 16.2 ± 5.1	0.1 ± 0.2	− 0.2 ± 0.7
DOPC	1.1 ± 0.2	0.6 ± 0.1	− 0.5 ± 0.1	0.0 ± 0.1

Fig. 3 shows representative AFM topographic images of homogeneous DOPC:DOTAP SLBs formed by VAR on SiO_2 recorded by QI-mode imaging at low force setpoint (Fig. 3A) and then evaluated as a function of time after exposure to QDs (Fig. 3 B-D). The supported bilayer seems quite homogeneous and rather defect-free. Force spectroscopy in a mapping mode was carried out to assess the membrane nanomechanics,

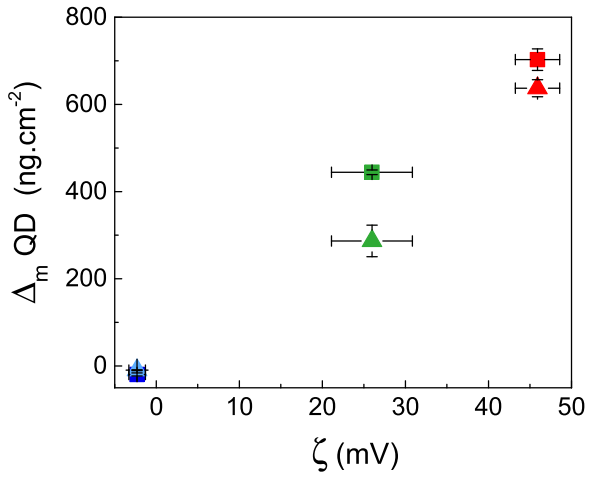

Fig. 2. Mass per unit area of hydrophilic CdTe QDs adsorbed onto homogeneous SLBs vs zeta-potential (ζ) of suspended vesicles of the same composition in bulk at 37 °C. Pure DOPC (blue), pure DOTAP (red), or DOPC:DOTAP (green). Supported lipid bilayers are represented by squares when formed by the VAR method, and by triangles when formed by the SALB method. (For interpretation of the references to colour in this figure legend, the reader is referred to the web version of this article.)

associated to the lateral organization, before and after addition of QDs. At long tip-surface vertical separation, no interaction is observed when the AFM tip approaches the SLB-covered SiO_2 surface until $d \sim 5$–6 nm, when repulsive interactions between the tip and the lipid molecules take over. From that point, the supported lipid layer is elastically compressed until the AFM tip punctures through the bilayer, reflected as the jump-in event in the approaching force distance curve. The vertical force at which this discontinuity takes place corresponds to the maximum force that the bilayer is able to withstand before breaking, commonly referred to as the breakthrough force (F_b) [30,31]. The frequency of force curves showing the above-described event in the mapped areas is similar before and after QDs adsorption. As a matter of fact, the shape of the curves barely changes (Fig. 3D), and the statistical analysis shows very similar breakthrough forces before and after QDs adsorption (Fig. 3C). After a certain time ($t < 16$ h) QDs at the used concentration do not significantly affect the nanomechanical stability of homogeneous supported lipid membranes. After prolonged exposure to QDs, we find that the breakthrough force decreases and thus the SLBs become laterally less organized. In fact, the probability of QD insertion into the bilayer likely might increase with time; however, we cannot rule out the role of possible flip-flop and bilayer degradation with time in the nanomechanical stability of the SLBs. Upon tip retraction, it is observed that the adhesion force increases with time. Adhesion between the tip and the SLB depends strongly on the approach velocity and the phase of the bilayer [32]. In our case, the approach velocity was kept constant and lipids within the bilayer are both in the liquid disordered phase at the measuring temperature. We are thus inclined to ascribe these changes to

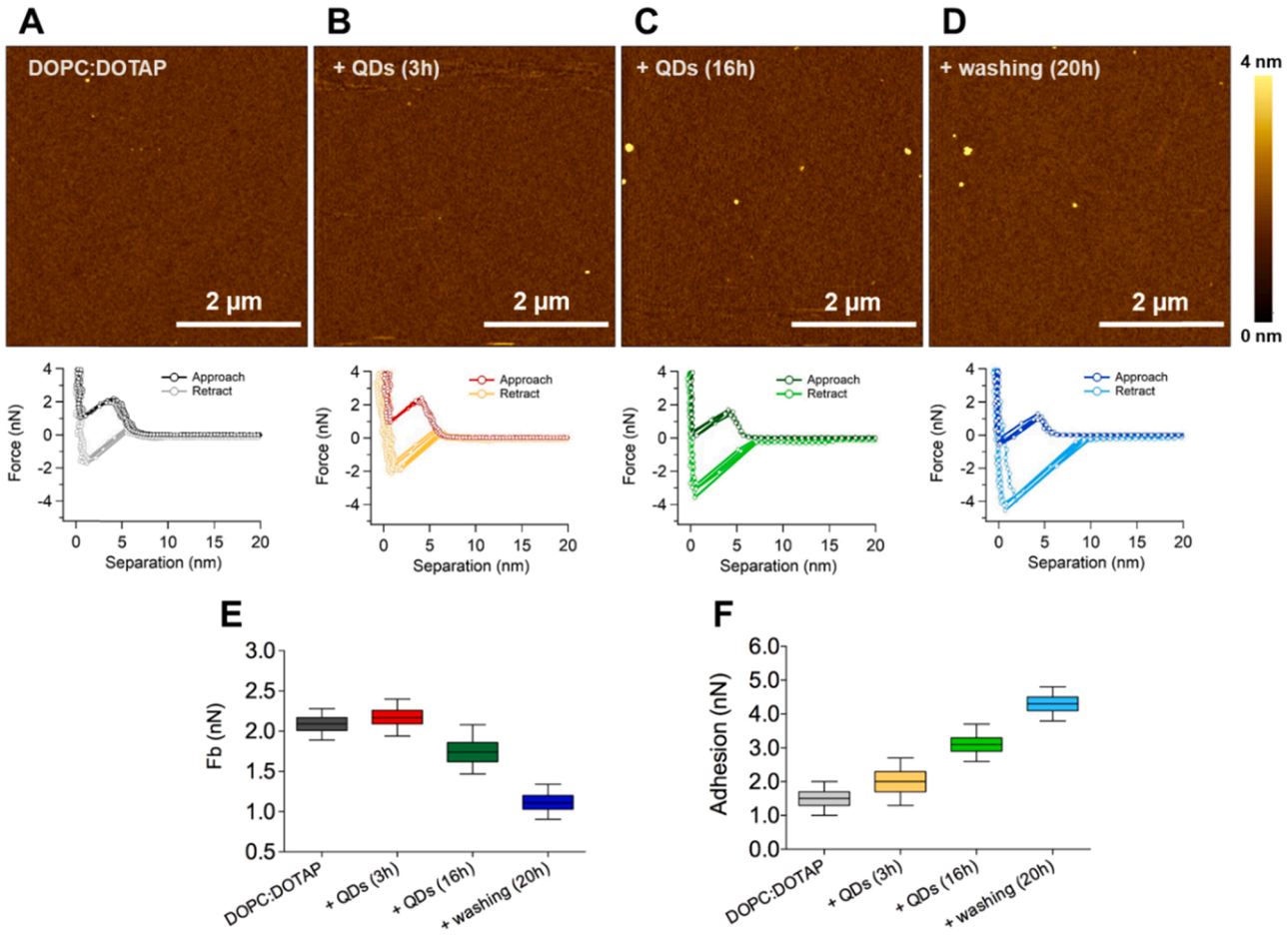

Fig. 3. Homogeneous DOPC:DOTAP SLBs (obtained by VAR) before and after addition of hydrophilic CdTe QDs monitored by QI-AFM as a function of time. AFM topographical images and examples of force vs. distance curves registered for (A) DOPC:DOTAP SLB, (B) after the addition of QDs (3 h), (C) after 16 h incubation, (D) after washing by buffer exchange, respectively. Scale bar: 2 µm. (E) Boxplot distribution of the corresponding breakthrough force values obtained from a statistical analysis of the approach part of multiple force vs distance curves ($800 < N < 1600$). (D) Adhesion values obtained from the retract part of the force curves.

partial insertion of the QDs, which would increase the disorder of the bilayer and thus induce a higher adhesion, as observed for SLBs with anaesthetic molecules that partition into the bilayer and increase the area per lipid [32].

3.2. QDs interactions with inhomogeneous -defect containing- supported lipid bilayers

In order to form inhomogeneous SLBs, SiO_2 surfaces with larger surface roughness (RMS $= 1.2 \pm 0.4$ nm) were used, based on recent findings reporting that nanoscale roughness strongly impacts the formation of homogeneous supported lipid bilayers [33]. Fig. 4 shows representative Δf/n and ΔD vs time responses upon the formation of inhomogeneous supported lipid membranes after the adsorption of DOPC:DOTAP and DOTAP vesicles and subsequent interactions with QDs. Unlike for homogeneous SLBs, both Δf/n and ΔD reach larger plateau values (in absolute value) and more importantly, the overtone signals do not overlap, indicating the presence of defects within the supported membranes that contribute to energy dissipation, i.e., unruptured vesicles and/or lipid patches with exposed edges. Upon the addition of QDs, the Δf/n and ΔD responses follow opposite behavior, Δf/n decreases (mass increases) reaching a stable plateau value, while ΔD displays a re-entrant behavior, with a fast small increase, followed by a large rapid decrease and a stable plateau. Overall, the mass over the sensor increases due to QD adsorption driven by electrostatic attraction (Δf/n increases in absolute value), yet rendering the layers more rigid and less dissipative as revealed by the fact that final ΔD response decreases and that final overtone plateaus overlap. This pattern of behavior can be rationalized as follows. Upon addition, the QDs first adsorb on the supported membranes by electrostatic attraction, and when present, also target defects where membrane curvature is enhanced, such as small unruptured vesicles or bilayer patch edges, yielding less dissipative layers by (local) vesicle rupture or edge insertion. In the case of DOPC:DOTAP mixtures, the overall frequency changes after QD addition are smaller than in DOTAP systems due to weaker electrostatic attraction. In turn, final dissipation plateau values are double for DOPC:DOTAP, indicating less efficient vesicle rupture due to weaker electrostatic attraction in the early stage of interaction and thus the presence of more layer defects such as unruptured vesicles, lipid multilayers and bare SiO_2 surface.

An alternative view of the QCM-D results for homogeneous and inhomogeneous SLBs can be seen in Fig. 5, which shows scaled frequency and dissipation shifts, $-\Delta f_n/f_n$ and $\Delta D_n/\pi$, as a function of the overtone number n. These two quantities account for the forces on the quartz (scaled with the quartz inertia) due to the adsorption of the lipids and QDs, the former being the inertial force, which is in phase with the quartz acceleration and the latter the friction force, which is in phase with the quartz velocity [34]. The formation of homogeneous films oscillating rigidly with the quartz surface is characterized by both quantities being overtone independent and by $\Delta D_n/\pi < -\Delta f_n/f_n$ [34]. In the case of homogeneous SLBs, the criterion is met for both quantities before and after QD addition. In the case of inhomogeneous SLBs, $-\Delta f_n/f_n$ first display clear overtone-dependent behavior. This phenomenon tends to weaken upon addition of QDs and is associated with less dissipative layers, which both guarantee a re-organization of the biomolecular layer.

Fig. 6 illustrates how the topography of the supported lipid membrane affects the hydrophilic QDs interactions with SLBs by comparing the change in dissipation on homogeneous and inhomogeneous supported membranes. The larger the dissipation of the underlying SLB (larger number of defects), the larger changes observed in this quantity upon QD addition. Likewise, the larger the dissipation of the SLB, the larger the decrease in frequency, confirming that QDs target primarily defects (see, for example, Fig. S2 in the Supplementary Material). In all cases, these changes lead to a dissipation decrease, where final values reach those we can find for classical homogeneous lipid bilayers. The insets in Fig. 6 display examples of AFM topography for DOPC:DOTAP and DOTAP SLBs corresponding to different values of dissipation obtained by QCM-D. Compared to homogeneous SLBs, inhomogeneous SLBs exposed to QDs exhibit a more complex topography, namely patches consisting of membrane multilayers (see ~~Material). On homogeneous (defect-free) supported membranes adsorption of QDs is electrostatically driven, the dissipation plateau does not change and the nanomechanical response is quite similar. On inhomogeneous supported membranes the interaction with QDs results from an interplay between initial electrostatic attraction and defect targeting. QDs target defect sites with enhanced curvature such as intact supported vesicles and exposed supported membrane edges. It has been reported that when QDs adsorb onto vesicles, strong adhesion takes over and wrapping of the vesicle membrane around the particle occurs, leading pore formation and lysis of the vesicles [35]. Supramolecular assembly of nanoparticles-lipid complexes driven by electrostatic and hydrophobic

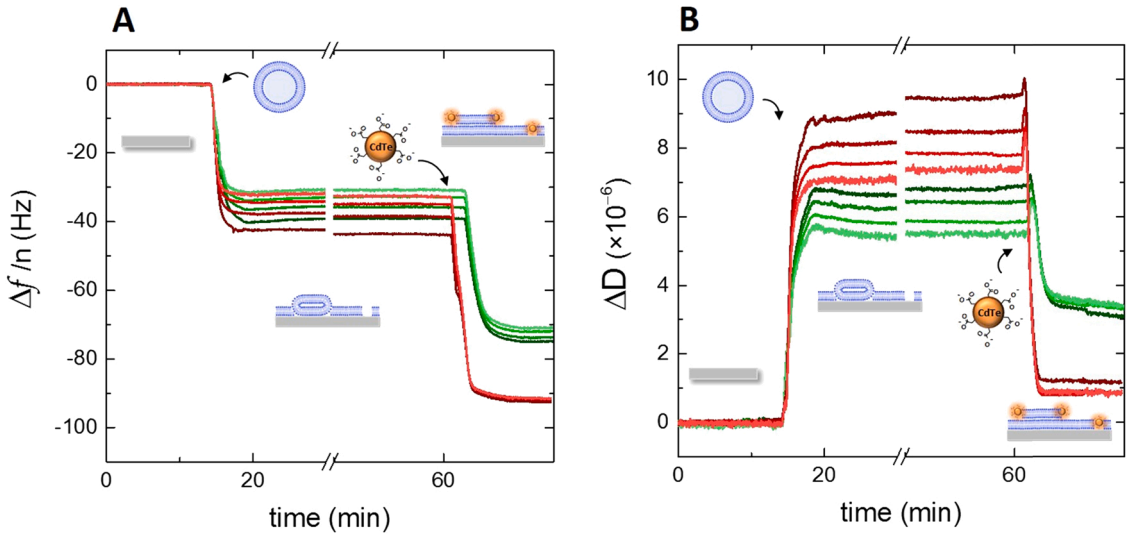

Fig. 4. Formation of inhomogeneous supported lipid layers by VAR on SiO_2 surfaces and subsequent interaction with hydrophilic CdTe QDs followed by QCM-D at 37 °C. Δf/n and ΔD changes recorded for overtones 3–9 are represented in panels A and B respectively. Red solid lines represent pure DOTAP data, green solid lines represent DOPC:DOTAP mixture data (colour gradient from darkest to brightest for overtone 3–9). (For interpretation of the references to colour in this figure legend, the reader is referred to the web version of this article.)

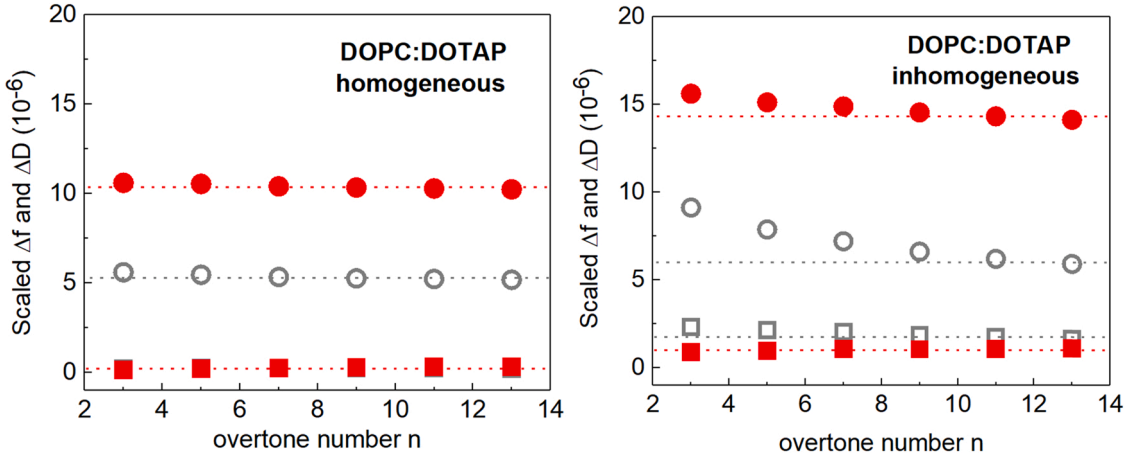

Fig. 5. Final scaled frequency (circles) and dissipation (squares) shifts as a function of the overtone number for homogeneous and inhomogeneous SLBs. Empty grey symbols refer to responses upon SLB formation, and red full symbols to subsequent adsorption of QDs. On the left panel, for homogeneous DOPC:DOTAP SLBs, grey and red squares overlap.(For interpretation of the references to colour in this figure legend, the reader is referred to the web version of this article.)

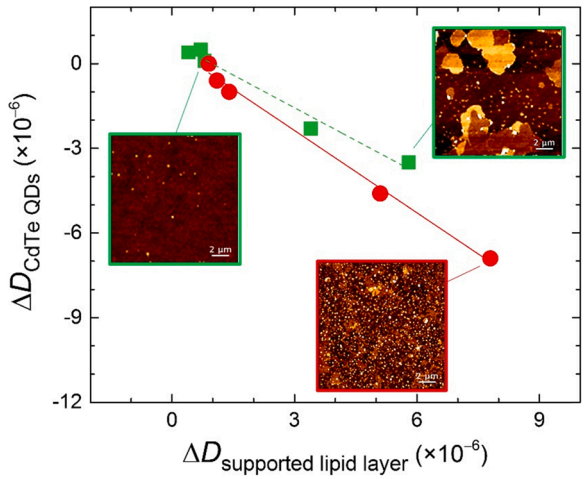

Fig. 6. Change in dissipation upon the addition of hydrophilic CdTe QDs as a function of the original dissipation of the DOPC:DOTAP (green) and DOTAP (red) supported lipid membranes on a SiO_2 sensor. Inset: Examples of AFM topographical images of homogeneous ($\Delta D_{\text{supported lipid bilayer}} \leq 0.5{\cdot}10^{-6}$) and inhomogeneous $\Delta D_{\text{supported lipid bilayer}} > 0.5{\cdot}10^{-6}$) SLBs upon the addition of QDs.

interactions has been shown for polyoxometalate nanoparticles leading to collapse of lipid vesicles and to lipid desorption [36]. In our case, vesicle rupture into supported lipid bilayers and multilayers took place within the timescale of the experiment, and subsequently added QDs were most likely inserted into the defects of the inhomogeneous supported membrane layers.

Overall, the addition of QDs has contributed to reducing the dissipation by i) vesicle rupture and formation of single bilayers and multilayers and ii) expulsion of buffer trapped within defects. A closer inspection of the patch boundary in both types of inhomogeneous SLBs after QD addition reveals that the layer thickness at the edges perimeter is higher, especially in case of DOTAP layers (see images in Fig. S4 of the Supplementary Material). The localized height increase can be attributed to CdTe QDs inserting into the edge of the lipid bilayer patch. Reference experiments showed that QDs do not adsorb to the bare SiO_2 surfaces due to electrostatic repulsion, indicating preferential interactions with the bilayer patch boundary (see Fig. S5 panel A in the Supplementary Material). Conversely, adsorption is observed on bare Au as shown in Fig. S5 panel B by QCM-D measurements and corresponding AFM images of the Au sensor where adsorption has taken place (Fig. S5 panel C). For a better visualization of QDs, they have been further adsorbed on an ultraflat Au surface resulting from template stripped chips from Platypus Technologies (Fig. S5 panel D).

We have compared the interactions of QDs onto DOPC and DOPC:DOTAP membranes formed on Au-coated quartz sensors, where, unlike for SiO_2 surfaces, adhesive energy is not strong enough to overcome the bending threshold for vesicle rupture and an intact vesicle layer is favored [22,37]. Fig. 7 shows a comparison of the QCM-D $\Delta f/n$ and ΔD responses upon DOPC and DOPC:DOTAP vesicle adsorption on Au-coated quartz sensors and subsequent addition of hydrophilic CdTe QDs. Both types of lipid vesicles exhibit a monotonous decrease of $\Delta f/n$ and increase of ΔD reaching large stable plateau values with non-overlapping overtones, indicating the formation of intact supported vesicle layers. The plateau values are larger in the case of DOPC vesicles, suggesting the presence of more intact, unruptured vesicles. Upon QDs addition, the ΔD signal decreases in both types of layers, QDs yield less dissipative layers by inducing local vesicle rupture. Noteworthy, the $\Delta f/n$ response displays an opposite pattern of behaviour, increasing for DOPC layers and decreasing for DOPC:DOTAP ones. When vesicles rupture, they release the buffer entrapped and form supported lipid bilayers and multilayers on the Au surface. The mass loss (represented by a $\Delta f/n$ increase) is counterbalanced by QD adsorption (represented by a $\Delta f/n$ decrease) in the case of DOTAP containing membranes due to attractive interactions. For pure DOPC membranes, vesicles are targeted and locally ruptured by QDs, releasing a larger amount of water. However, due to repulsive interactions with the (locally) formed SLBs QDs do not adsorb onto the resulting bilayers.

4. Conclusions

We have used QCM-D to monitor the interactions between hydrophilic, negatively charged CdTe quantum dots with solid-supported lipid bilayers (SLBs) focusing on the effect of SLB surface charge and topographical inhomogeneities. Two different strategies were carried out to form SLBs, namely vesicle adsorption and rupture (VAR), and solvent assisted lipid bilayer formation (SALB). AFM was used as a complementary tool to confirm the two last points.

The formation pathway of homogeneous bilayers ($\Delta D \leq 0.5.10^{-6}$) on a SiO_2 surface using VAR depends strongly on the vesicle's zeta potential. The more positively the vesicles are charged (DOPC < DOPC:DOTAP < DOTAP), the fewer adsorbed vesicles required for fusion and rupture, eventually rupturing immediately upon adsorption in the case of positively charged DOTAP vesicles. SALB using the same kind of lipids yielded values of frequency and dissipation responses similar to those by

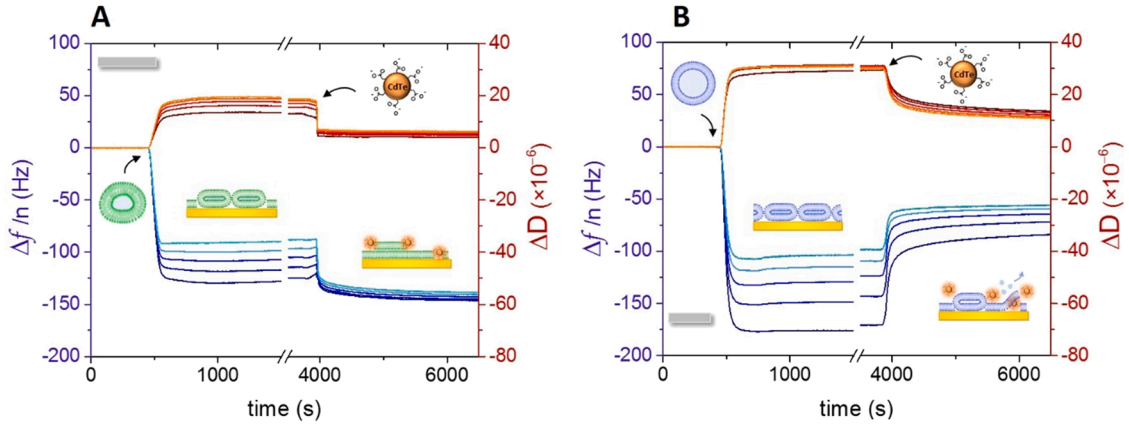

Fig. 7. Formation of inhomogeneous DOPC:DOTAP (A) and pure DOPC (B) supported lipid layers by VAR on Au and subsequent interaction with hydrophilic CdTe QDs followed by QCM-D at 37 °C. Δ*f*/n and Δ*D* changes recorded for overtones 3–9 are represented in panels A and B respectively (colour gradient from darkest to brightest for overtone 3–9).

VAR and commensurate with the formation of homogeneous, rigid SLBs onto SiO_2 surfaces. Concerning the adsorption of QDs, the proportionality observed between frequency shifts and the vesicles zeta potential indicates that the interaction is driven by electrostatic attractions, while the stability of the dissipation signals within the timescale of the QCM-D experiments suggests that QDs adsorb and do not (globally) disturb the supported bilayers. QDs adsorbed onto DOPC:DOTAP SLBs formed by SALB and VAR points towards the more asymmetric character of the former. AFM topographical imaging confirm topographically homogeneous bilayers, displaying similar nanomechanical responses before and after QD addition. After prolonged QD exposure, the nanomechanical stability of the SLBs decreases and the adhesion strength between the SLB and the AFM tip increases, due to an enhanced probability of bilayer reorganization and of nanoparticle insertion.

The presence of inhomogeneities in SLBs was evaluated using the QCM-D dissipation values and overtone dispersion as descriptors. The differences in frequency and dissipation changes upon QDs addition with respect to their homogeneous SLB counterparts reveal that, apart from electrostatic interactions, QDs interactions with inhomogeneous SLBs are also driven by defect targeting. As a matter of fact, the more inhomogeneous the SLB, the more QDs adsorb, inducing vesicle rupture and insertion at patch edges, as revealed by AFM imaging.

These results show the importance of supported membrane topography in the interactions with nanoparticles and provide experimental evidence that, apart from electrostatic attraction, nanoparticle interactions are also modulated by the presence of defects, i.e., unruptured vesicles and edges with enhanced curvature. The information provided can motivate further studies on fundamental mechanisms for defect-mediated QD uptake in more complex biological environments and help towards the design of nanoparticles with specific cytotoxic effects.

CRediT authorship contribution statement

L. Bar: QCM-D, DLS, contact angle and AFM data acquisition and analysis, **F. Perissinotto**: AFM data acquisition and analysis, **L. Redondo-Morata**: Methodology, data analysis, reviewing, editing, and fund raising **M.I. Giannotti**: Methodology, data analysis, reviewing editing, and fund raising. **J. Goole:** DLS data acquisition and methodology. **P. Losada-P é rez**: conceptualization, supervision, writing – reviewing & editing and fund raising.

Declaration of Competing Interest

The authors declare that they have no known competing financial interests or personal relationships that could have appeared to influence the work reported in this paper.

Acknowledgments

This research was funded by the Fonds de la Recherche Scientifique (FNRS) Project MIS under grant number F.4525.20. and the Université Libre de Bruxelles (ULB), Project ARC grant number 20061. L.R.M. acknowledges funding from the Agence National de la Recherche (ANR), as part of the 'Investments d'Avenir' Program (I-SITE ULNE/ANR-16-IDEX-0004 ULNE). M.I.G. acknowledges the Agency for Management of University and Research Grants/Generalitat de Catalunya (CERCA Programme, 2017-SGR-1442).

Appendix A. Supporting information

Supplementary data associated with this article can be found in the online version at doi:10.1016/j.colsurfb.2021.112239.

References

[1] M. Chu, X. Pan, D. Zhang, Q. Wu, J. Peng, W. Hai, The therapeutic efficacy of CdTe and CdSe quantum dots for photothermal cancer therapy, Biomaterials 33 (2012) 7071–7083.
[2] C.T. Matea, T. Mocan, F. Tabaran, T. Pop, O. Mosteanu, C. Puia, C. Iancu, L. Mocan, Quantum dots in imaging, drug delivery and sensor applications, Int. J. Nanomed. 12 (2017) 5421–5431.
[3] R. Tero, Substrate effects on the formation process, structure and physicochemical properties of supported lipid bilayers, Materials 5 (2012) 2658–2680.
[4] G.J. Hardy, R. Nayak, S. Zauscher, Model cell membranes: techniques to form complex biomimetic supported lipid bilayers via vesicle fusion, Curr. Opin. Colloid Interface Sci. 18 (2013).
[5] E.C. Cho, L. Au, Q. Zhang, Y. Xia, The effects of size, shape, and surface functional group of gold nanostructures on their adsorption and internalization by cells, Small 6 (2010) 517–522.
[6] Y. Roiter, M. Ornatska, A.R. Rammohan, J. Balakrishnan, D.R. Heine, S. Minko, Interaction of nanoparticles with lipid membrane, Nano Lett 8 (2008) 941–944.
[7] T. Hamada, M. Morita, M. Miyakawa, R. Sugimoto, A. Hatanaka, M.C. Vestergaard, M. Takagi, Size-dependent partitioning of nano/microparticles mediated by membrane lateral heterogeneity, J. Am. Chem. Soc. 134 (2012) 13990–13996.
[8] B. Lu, T. Smith, J.J. Schmidt, Nanoparticle–lipid bilayer interactions studied with lipid bilayer arrays, Nanoscale 7 (2015) 7858–7866.
[9] S. Tatur, M. Maccarini, R. Barker, A. Nelson, G. Fragneto, Effect of functionalized gold nanoparticles on floating lipid bilayers, Langmuir 29 (2013) 6606–6614.
[10] R.C. Van Lehn, P.U. Atukorale, R.P. Carney, Y.-S. Yang, F. Stellacci, D.J. Irvine, A. Alexander-Katz, Effect of particle diameter and surface composition on the spontaneous fusion of monolayer-protected gold nanoparticles with lipid bilayers, Nano Lett 13 (2013) 4060–4067.
[11] E. Canepa, S. Salassi, F. Simonelli, R. Ferrando, R. Rolandi, C. Lambruschini, F. Canepa, S. Dante, A. Relini, G. Rossi, Non-disruptive uptake of anionic and cationic gold nanoparticles in neutral zwitterionic membranes, Sci. Rep. 11 (2021) 1256.
[12] R.C.V. Lehn, A. Alexander-Katz, Pathway for insertion of amphiphilic nanoparticles into defect-free lipid bilayers from atomistic molecular dynamics simulations, Soft Matter 11 (2015) 3165–3175.
[13] E. Heikkilä, H. Martinez-Seara, A.A. Gurtovenko, M. Javanainen, H. Häkkinen, I. Vattulainen, J. Akola, Cationic au nanoparticle binding with plasma membrane-

like lipid bilayers: potential mechanism for spontaneous permeation to cells revealed by atomistic simulations, J. Phys. Chem. C. 118 (2014) 11131–11141.
[14] R.C.V. Lehn, A. Alexander-Katz, Energy landscape for the insertion of amphiphilic nanoparticles into lipid membranes: A computational study, PLOS ONE 14 (2019).
[15] R.C. Van Lehn, M. Ricci, P.H.J. Silva, P. Andreozzi, J. Reguera, K. Voïtchovsky, F. Stellacci, A. Alexander-Katz, Lipid tail protrusions mediate the insertion of nanoparticles into model cell membranes, Nat. Commun. 5 (2014) 4482.
[16] A.C. Mensch, E.S. Melby, E.D. Laudadio, I.U. Foreman-Ortiz, Y. Zhang, A. Dohnalkova, D. Hu, J.A. Pedersen, R.J. Hamers, G. Orr, Preferential interactions of primary amine-terminated quantum dots with membrane domain boundaries and lipid rafts revealed with nanometer resolution, Environ. Sci. Nano 7 (2020) 149–161.
[17] A.S. Ulrich, M. Sami, A. Watts, Hydration of DOPC bilayers by differential scanning calorimetry, Biochim. Biophys. Acta - Biomembranes 1191 (1994) 225–230.
[18] T. de, P. Rigoletto, C.L. Silva, M.H.A. Santana, R.S. Rosada, L.G. de la Torre, Effects of extrusion, lipid concentration and purity on physico-chemical and biological properties of cationic liposomes for gene vaccine applications, J. Microencapsul. 29 (2012) 759–769.
[19] S.R. Tabaei, J.A. Jackman, S.-O. Kim, V.P. Zhdanov, N.-J. Cho, Solvent-assisted lipid self-assembly at hydrophilic surfaces: factors influencing the formation of supported membranes, Langmuir 31 (2015) 3125–3134.
[20] S.R. Tabaei, J.-H. Choi, G. Haw Zan, V.P. Zhdanov, N.-J. Cho, Solvent-assisted lipid bilayer formation on silicon dioxide and gold, Langmuir 30 (2014) 10363–10373.
[21] P. Losada-Pérez, O. Polat, A.N. Parikh, E. Seker, F.U. Renner, Engineering the interface between lipid membranes and nanoporous gold: A study by quartz crystal microbalance with dissipation monitoring, Biointerphases 13 (2018), 011002.
[22] R. Lipowsky, U. Seifert, Adhesion of vesicles and membranes, Mol. Cryst. Liq. Cryst. 202 (1991).
[23] E.-L. Florin, M. Rief, H. Lehmann, M. Ludwig, C. Dornmair, V.T. Moy, H.E. Gaub, Sensing specific molecular interactions with the atomic force microscope, Biosens. Bioelectron. 10 (1995) 895–901.
[24] C.A. Keller, B. Kasemo, Surface specific kinetics of lipid vesicle adsorption measured with a quartz crystal microbalance, Biophys J 75 (1998) 1397–1402.
[25] N.J. Cho, C.W. Frank, B. Kasemo, F. Höök, Quartz crystal microbalance with dissipation monitoring of supported lipid bilayers on various substrates, Nat Protoc 5 (2010) 1096–1106.
[26] R. Richter, A. Mukhopadhyay, A. Brisson, Pathways of lipid vesicle deposition on solid surfaces: a combined QCM-D and AFM Study, Biophys. J. 85 (2003) 3035–3047.
[27] X. Zhang, S. Yang, Nonspecific adsorption of charged quantum dots on supported zwitterionic lipid bilayers: real-time monitoring by quartz crystal microbalance with dissipation, Langmuir 27 (2011) 2528–2535.
[28] G. Sauerbrey, Verwendung von schwingquarzen zur wägung dünner schichten und zur mikrowägung, Z. Physik 155 (1959) 206–222.
[29] I. Reviakine, D. Johannsmann, R.P. Richter, Hearing what you cannot see and visualizing what you hear: interpreting quartz crystal microbalance data from solvated interfaces, Anal. Chem. 83 (2011) 8838–8848.
[30] Y.F. Dufrêne, W.R. Barger, J.-B.D. Green, G.U. Lee, Nanometer-scale surface properties of mixed phospholipid monolayers and bilayers, Langmuir 13 (1997) 4779.
[31] L. Redondo-Morata, P. Losada-Pérez, M.I. Giannotti, Chapter one - lipid bilayers: phase behavior and nanomechanics, in: I. Levitan, A. Trache (Eds.), Current Topics in Membranes, Academic Press, 2020, pp. 1–55.
[32] Z. Leonenko, E. Finot, D. Cramb, AFM study of interaction forces in supported planar DPPC bilayers in the presence of general anesthetic halothane, Biochim. Biophys. Acta - Biomembranes. 2006 (1758) 487–492.
[33] F. Blachon, F. Harb, B. Munteanu, A. Piednoir, R. Fulcrand, T. Charitat, G. Fragneto, O. Pierre-Louis, B. Tinland, J.-P. Rieu, Nanoroughness Strongly Impacts Lipid Mobility in Supported Membranes, Langmuir 33 (2017) 2444–2453.
[34] J.J.J. Gillissen, S.R. Tabaei, N.-J. Cho, A phenomenological model of the solvent-assisted lipid bilayer formation method, Phys. Chem. Chem. Phys. 18 (2016) 24157–24163.
[35] S. Zuraw-Weston, D.A. Wood, I.K. Torres, Y. Lee, L.-S. Wang, Z. Jiang, G.R. Lázaro, S. Wang, A.A. Rodal, M.F. Hagan, V.M. Rotello, A.D. Dinsmore, Nanoparticles binding to lipid membranes: from vesicle-based gels to vesicle tubulation and destruction, Nanoscale 11 (2019) 18464–18474.
[36] H. Nabika, A. Sakamoto, T. Motegi, R. Tero, D. Yamaguchi, K. Unoura, Imaging characterization of cluster-induced morphological changes of a model cell membrane, J. Phys. Chem. C. 120 (2016) 15640–15647.
[37] S.K. Pramanik, S. Seneca, A. Ethirajan, S. Neupane, F.U. Renner, P. Losada-Pérez, Ionic strength dependent vesicle adsorption and phase behavior of anionic phospholipids on a gold substrate, Biointerphases 11 (2016), 019006.